Fluid Phase Equilibria 516 (2020) 112615

Contents lists available at ScienceDirect

Fluid Phase Equilibria

journal homepage: www.elsevier.com/locate/fluid

Molecular dynamics simulation on Na^+-F^- ion-pair association from ambient to supercritical water

Wei Zhang [a, *], Tinggui Yan [b]

[a] Research Center of Karst Ecological Civilization, Guizhou Normal University, Guiyang, 550025, China
[b] School of Chemistry and Chemical Engineering, Guizhou University, Guiyang, 550025, China

ARTICLE INFO

Article history:
Received 28 January 2020
Received in revised form
15 April 2020
Accepted 17 April 2020
Available online 4 May 2020

Keywords:
Na^+-F^- ion pair
Molecular dynamics
Potential of mean force (PMF)
Association constant

ABSTRACT

Constrained classical molecular dynamics simulations were carried out to investigate the sodium fluoride associations in dilute aqueous solutions from ambient to supercritical thermodynamic condition. Solvent mediated potential of mean force (PMF) of Na^+-F^- ions pair was calculated by thermodynamic integration with five different force fields and the SPC/E water model. The corresponding association constants were also calculated from the PMFs. The structure and dynamics of Na^+ and F^- in water calculated from these force fields were compared with the results from *ab initio* molecular dynamics at 298 K. The results show Na^+-F^- ion-pair tends to associate with increasing temperature and dissociate with increasing pressure. The association constants of the ion-pairs (K_{all}) including contact ion-pair (CIP), solvent shared ion-pair (SShIP) and solvent separated ion-pair (SSIP) from different force fields agreed well with each other within 0.4 log unit in the whole thermodynamic condition, and they are also in accordance with the recently published data at 298 K. But in the sub-supercritical region, significant deviations occurred between the contact ion-pair association constants (K_{CIP}) and K_{all} for each force field and also between K_{CIP} from different force fields. These two kinds of deviations decreased at higher temperature when CIP became the predominated configuration. Comparison of radial distribution functions (RDFs) characteristics from the five force fields with that from AIMD calculation shows that the force field parameters developed by combing single ion properties with mineral lattice energy or ion-pair interaction properties is better.

1. Introduction

Ion-pair association in high temperature and pressure solution is an important subject for hydrothermal technologies and hydrothermal geochemistry [1,2]. Ion-pair association constants are needed to predict the ion speciation, which is essential to correlate the solubility of electrolytes in sub-to supercritical water, or to examine the hydrothermal ore formation processes [3–5].

Fluoride is widely dispersed in nature hydrothermal geofluid, and it plays a significant role in metal element hydrothermal mobilization and transportation for the formation of fluoride complexes [6,7]. NaF is probably the dominant fluoride salt in geofluids, and its association restricts the migration and conversion of fluoride, the speciation which is of great significance for evaluating the migration and enrichment of ore-forming elements [8,9].

The presence of sodium fluoride association in aqueous solutions has been proved by many experimental studies [10–13]. Using the experimental solubility data of NaF salt, Faridi and El Guendouzi [10] and Aghaie and Samaie [11] found ion-association is the reason for the greater value of experimental thermodynamic solubility product over that calculated from standard Gibbs energy. Their association constants (K_a) at 298 K were 1.675 and 1.864, respectively. However, the values of K_a at 298 K from previous publications summarized by Majer et al. [14] varies from 0.11 to 1.07. In addition, there are no directly experimental studies on sodium fluoride association at high temperature and pressure. Majer et al. [14] indirectly estimated Na^+-F^- ion pair association constants at temperature up to 625 K and pressure up to 300 bar from NaF volumetric properties. Richardson and Holland [15] indirectly estimated it via fitting experimental fluorite solubility data in NaCl solution at temperature up to 533 K and saturated vapor pressure.

Molecular dynamics (MD), another important means to study the association behavior of electrolyte solutions, is complementary to

* Corresponding author.
E-mail address: zhangwei2011@hotmail.com (W. Zhang).

https://doi.org/10.1016/j.fluid.2020.112615
0378-3812/

experiments and can provide a detailed molecular picture of the ion pairs [16]. Ion-pair association constants could be calculated from the MD obtained potential of mean force (PMF). This PMF approach has been successfully applied for the studying the ion association behavior of sodium chloride [17–19], alkaline-earth metal halide complexes [20–23], divalent metal sulfate complexes [24], and divalent metal nitrate complexes [25] in sub-to supercritical water. Fennell et al. [26] investigated Na^+–F^- association with different force fields at 298 K. Three ion-pair configurations of the contact ion pair (CIP), solvent shared ion pair (SShIP) and solvent separated ion pairs (SSIP) were found and confirmed by the dielectric relaxation experiments [27]. But there is little MD research on Na^+–F^- association under hydrothermal conditions despite the critical importance.

The ion-pair association constants calculated by classical molecular simulation are force fields sensitive [26]. Recently, there have been many attempts to develop force fields for alkali metals and halide ions, including Na^+–F^- pair. Koneshan et al. [28] parametrized Na^+–F^- empirical force fields based on single ion properties of the binding energies of small clusters of ions with SPC/E [29] water models. However, force fields based on single ion properties often fail to reproduce realistically the ion-ion fluid structure and thermodynamics of the electrolytes [30,31]. Joung and Cheatham [32] have used the free energy of hydration for individual ions, as well as the lattice energies and the lattice constants of alkali metal halides and the gas phase ion-water interaction energies to produce force fields for all of the alkali metal and halide ions with SPC/E, TIP3P, and $TIP4P_{EW}$ water models. But, Gee et al. [33] argued that they were not directly probing ion-ion interactions in solution.

The Kirkwood-Buff [34] theory, providing a link between the thermodynamic properties of a solution, such as derivatives of the chemical potentials, osmotic pressure, partial molar volumes, and underlying molecular distributions, has been widely used to develop the Kirkwood-Buff derived force fields for Na^+–F^- in conjunction with the SPC/E water model. Gee et al. [33] used the experimental available activity coefficients and solution densities to produce force fields of Na^+ and F^-. Fyta and Netz [35] optimized their ionic force fields based on single-ion solvation free energy and the finite-concentration osmotic pressure as benchmarks. Deublein et al. [36] developed force fields parameters of Na^+ and F^- with the reduced liquid solution density. It is unclear which of these force field parameters would give the accurate association behavior of sodium fluoride.

The main objective of the present study is to evaluate Na^+–F^- association behavior from ambient to supercritical water by classical molecular dynamic. To get that, the above mentioned five force field parameters from Koneshan et al. [28], Joung and Cheatham [32], Gee et al. [33], Fyta and Netz [35], Deublein et al. [36] were employed with SPC/E water model to calculate sodium fluoride PMF. And the association constant of Na^+–F^- ion pair (K_a) were calculated with the PMFs. The prediction capacity of these force fields is tested by comparing the MD calculated K_a with experimental data, and by comparing the structure and dynamics of Na^+ and F^- in water from these force fields with the results from *ab initio* molecular dynamics at 298 K.

In Section 2 of the present paper, the computational methodology and employed force fields are described. In Section 3, the simulated results are presented and discussed. Section 4 summarizes the main statement from the present work.

2. Method

2.1. Association constants and potential of mean forces

Ion pairing is described as the association of oppositely charged ions in electrolyte solutions to form distinct physicochemical species. This forming process is stepwise when these ions coming close to each other:

$$A^- + C^+ \rightarrow A^-||C^+ \rightarrow A^-|C^+ \rightarrow A^-C^+ \tag{1}$$

$$K_a = \frac{a_{(A:C)}}{a_A a_C} = \frac{c_{(A:C)}\gamma_{(A:C)}}{c_A c_C \gamma_{\pm}^2} \tag{2}$$

where A^- and C^+ are free cation and anion ions, | stands for solvent molecule. $A^-||C^+$ is SSIP, where both the cation and anion retain one full hydration shell and the ions are separated by two solvent molecules; $A^-|C^+$ is SShIP, where the cation and anion are separated by one shared water molecule; A^-C^+ is CIP, where the cation and anion are in direct contact with each other. K_a is the ion pair association constant, a_i, c_i and γ_i are the activity, concentration and activity coefficient of the species i, respectively. A:C is the associated ion pair, $\gamma_{(A:C)}$ is the corresponding activity coefficient. $\gamma_{\pm}$ is the mean activity coefficient of the free ions in solution.

The free energy of A^- and C^+ along the reaction coordinate is known as the potential of mean force (PMF). The association constants can be calculated from the PMF [37]:

$$K_a = 4\pi R \int_0^{r_c} \exp\left(\frac{-W(r)}{k_B T}\right) r^2 \mathrm{d}r \tag{3}$$

where $W(r)$ is the PMF along the pathway as a function of ionic separation r, r is the separated distance between the cation and anion ions, r_c is the interionic distance of criterion dividing the "associated ion-pair" and "free ions". k_B is Boltzmann constants, T is the absolute temperature, $R = N_A \times 10^{-24}$ (N_A is the Avogadro number), is the conversion factor to convert the unit of K_a from nm^3/molecule to L/mol ($K_a(M)$).

The values of r_c are variable with the definition of the associated ion-pair. There are two different conjectured definitions of associated ion-pair. The first one only treats the direct contact ion pair CIP as associated ion-pair [38–40], while the second also takes the water shared and separated configuration into calculation, i.e. associated ion-pair = CIP + SShIP + SSIP [3,37,41–43]. In this work, K_a was calculated using both definitions.

The simulation method was adopted from the references (we mainly referred the work of Chialvo and coworkers [37,42–44]). This MD PMF methodology is widely used [3,4,19,38,41]. During the constrained MD calculation, the cation-anion distance is fixed at certain separation r, and the average effective force $F(r)$ is determined from the accumulative average of the sampled constraint force. Then, the $W(r)$ between the anion and the cation is calculated via the thermodynamic integration [38,45]:

$$W(r) = W(r_0) - \int_{r_0}^{r} F(r)\mathrm{d}r \tag{4}$$

where r_0 is the distance at a reference state where the inter-ionic distance is long enough and $W(r_0)$ can be assumed to be the effective potential between ions in continuum medium:

$$W(r_0) = \frac{1}{4\pi}\frac{q_A q_C}{\varepsilon r_0} \tag{5}$$

where q_A and q_C are the charges of the anion and cation ions, ε is the solvent dielectric constant of water and calculated from the equations of Plugatyr and Svishchev [46]. r_0 was set to be 1 nm. The relative population of CIP configuration can also be calculated [24,47]:

$$P_{CIP} = \frac{[\mathrm{CIP}]}{[\mathrm{CIP} + \mathrm{SShIP} + \mathrm{SSIP}]} = \frac{\int_0^{r_{CIP}} \exp\left(\frac{-W(r)}{k_B T}\right) r^2 \mathrm{d}r}{\int_0^{r_c} \exp\left(\frac{-W(r)}{k_B T}\right) r^2 \mathrm{d}r} \quad (6)$$

where $[\cdots]$ denotes mole concentration of the configurations.

2.2. Classical MD simulation details

The software Gromacs version 5.1 [48] was used for all the classical MD calculation. The intermolecular interactions are described by the Lennard-Jones (LJ) and Coulomb potentials:

$$u_{ij} = 4\varepsilon_{ij}\left[\left(\frac{\sigma_{ij}}{r_{ij}}\right)^{12} - \left(\frac{\sigma_{ij}}{r_{ij}}\right)^{6}\right] + \frac{q_i q_j}{4\pi\varepsilon_0 r_{ij}} \quad (7)$$

where u_{ij} is the potential energy between the particles i and j with a distance r_{ij} between their LJ sites. σ_{ij} and ε_{ij} are the LJ parameters for size and energy, respectively; q_i and q_j are the charges of the solute or the solvent particles, and ε_0 is the vacuum permittivity.

The simple point charge extended (SPC/E) model for water was employed. Force field parameters of Na^+ and F^-, summarized in Table 1, were adopted from literature of Koneshan et al. [28] (referred as the ff_KRLL), Fyta and Netz [35] (ff_FN), Joung and Cheatham [32] (ff_JC), Deublein et al. [36,49] (ff_DRVH) and Gee et al. [33] (ff_GCJBWS). The Lorentz-Berthelot combination rules were used for the LJ parameters of ff_KRLL, ff_JC, ff_DRVH. For the force field of ff_FN, a specified scaling factor of 1.5 was applied for the Na^+–F^- LJ ε parameter according to $\varepsilon_{NaF} = 1.5\sqrt{\varepsilon_{Na}\varepsilon_F}$. The geometric combination rules were used for the σ and ε parameters of ff_GCJBWS, and the Na-oxygen ε parameter was then modified using a Na^+ specified scaling factor of 0.75 such that $\varepsilon_{NaO} = 0.75\sqrt{\varepsilon_{Na}\varepsilon_O}$.

During classical MD simulation, the geometry of the water molecules was fixed by means of the SETTLE algorithm [50], and the distance between Na^+ and F^- was kept by LINCS algorithm [51]. The leap-frog algorithm [52] with a time step of 2 fs was used to integrate the equations of motion. Periodic boundary conditions were applied in all three directions. The temperature and pressure of the simulation systems were controlled by using the Nosé-Hoover thermostat [53,54] and Parrinello–Rahman barostat [55] with the time constants of 0.5 ps and 1.0 ps, respectively. The cut-off for both non-bonded van der Waals and Coulomb interactions was 1.0 nm. The electrostatic interactions were treated by PME method [56].

Simulations of constrained classical MD were performed with 518 water molecules and 1 Na^+–F^- ion pair. Temperature of the simulated system was in the range of 298 K–873 K with pressure ranging from 1 bar to 1000 bar. The comparisons of those five force field parameters were conducted at three thermodynamic conditions: 298 K and 1 bar, 523 K and 500 bar and 773 K and 1000 bar. The finite size effects were estimated at 523 K and 500 bar with 300, 518 and 1036 water molecules by using force fields of ff_KRLL. For each constrained MD simulation, the Na^+–F^- ion-pair separation started from 0.2 nm and extended up to 1.2 nm with a separation step of 0.01 nm for the range of 0.20–0.80 nm, and a step of 0.02 nm for the range of 0.80–1.20 nm. For each interionic separation simulation, the systems were equilibrated for 2 ns isothermal-isobaric (NPT) ensemble, following by production of 4 ns canonical constant volume (NVT) ensemble for separation distance less than 0.6 nm, and 8 ns NVT simulation for separation distance greater than 0.6 nm.

Table 1
Lennard-Jones and Electrostatic parameters for the ions and SPC/E water force fields.

		ε_{ii} (kJ/mol)	σ_{ii} (nm)	ε_{iO} (kJ/mol)	σ_{iO} (nm)
Ff_KRLL	Na	0.5216	0.2876		
	F	0.6998	0.3143		
ff_JC	Na	1.4754	0.2160		
	F	0.0310	0.4022		
ff_FN	Na	0.4186	0.2583	0.5216	0.2876
	F	0.4161	0.0150	0.1000	0.3665
	Na–F	0.1189	0.3372		
ff_GCJBWS	Na	0.3200	0.2450	0.3420	
	F	1.0000	0.3700		
Ff_DRVH	Na	1.6629	0.1890		
	F	1.6629	0.3660		
SPC/E	O	0.6502	0.3166		
	H	0.0000	0.0000		

2.3. AIMD simulation details

The *ab initio* molecular dynamics (AIMD) were performed using the hybrid Gaussian plane wave approach employed freely available CP2K/QUICKSTEP package [57]. The AIMD simulations were performed with the NVT ensemble using a time step of 0.5 fs, and employing the periodic boundary conditions in a box of 12.6 × 12.6 × 12.6 Å containing one sodium-fluoride pair and 64 water molecules. The temperature of 298 K was maintained using the Nosé-Hoover thermostat with a time constant of 0.5 fs. The B3LYP [58,59] density function level was employed with the Grimme correction scheme to account for dispersion interactions [60] (B3LYP-D3). Kohn-Sham orbitals were expanded in a Gaussian basis set (TZV2P MOLOPT for O, H, and F and DZVP MOLOPT for Na) [61], and the Goedecker-Teter-Hutter pseudopotentials [62] were used to avoid the core state calculation. The electron density was expanded in an auxiliary basis set with a plane-wave cutoff of 400 Ry [21]. The production simulation was running for 15.0 ps following an equilibration for 4.0 ps.

2.4. Association constant uncertainties estimation

The uncertainties of the PMF and $\log_{10}K_a$ were calculated by standard propagation rules from the statistical error of the average effective force $F(r)$. And the statistical error of $F(r)$ was estimated following the method demonstrated by Allen and Tildesley [63], which has been successfully used for example by Zhang and Duan [41] and Mei et al. [38]:

$$\sigma_{mean} = \sqrt{\frac{s}{n}}\sigma \quad (8)$$

$$\sigma^2 = \frac{1}{n}\sum_{n=1}^{n} \left(f(r)_t - \bar{f}(r)\right)^2 \quad (9)$$

where σ is the standard deviation of the mean force $F(r)$, n is the number of samples (time steps) collected in a given run. $f(r)$ and $\bar{f}(r)$ are the force at tth time step and mean force of that run, respectively. s is the statistical inefficiency introduced during the highly correlated successive force recording process. It is estimated according to:

$$s = \lim_{n_b \to \infty} n_b \frac{\sigma_b^2}{\sigma^2} \quad (10)$$

where n_b and σ_b are the number of samples and standard deviation of a single block, respectively. The total number of samples (n) is

divided into several blocks with the length of n_b for each block.

The standard deviation of the mean force σ and the statistical inefficiency s are estimated independent in each simulation. The statistical errors of PMF and $\log_{10}K_a$ are calculated by uncertainties propagation from the accumulating σ_{mean} of $F(r)$ over the thermodynamic integration using Eq. (3) and Eq. (4).

3. Results and discussion

3.1. PMF comparison of these force field

The PMF profiles of Na^+–F^- ion-pair calculated with these force field parameters at the three comparing thermodynamic conditions were shown in the left part of Fig. 1. Each of the free energy profiles exhibits three local minima that corresponding to three different types of ion-pair configurations: CIP (~0.25 nm), SShIP (~0.45 nm) and SSIP (~0.65 nm). The positions and intensity of these configurations vary slightly from each other. At 298 K, the position of the CIP changes from 0.24 nm to 0.26 nm as moving from ff_JC to ff_KRLL, and the PMF values of the CIP are varying from 5.090 kJ/mol to −3.562 kJ/mol when moving from the ff_FN to the ff_KRLL force fields (Fig. 1a(1)).

The PMF values of CIP, SShIP and SSIP also reflect the stability of the configurations. The formation of CIP from SShIP requires the removal of a water molecule from the first hydration shell of the metal to accommodate the associating anion [20,21] (Fig. S1). At 298 K, the CIP PMF values calculated by ff_FN, ff_JC and ff_GCJBWS are larger than those SShIP, and the transition energy barriers from CIP to SShIP are much smaller than those from SShIP to CIP, which means SShIP configuration is the more stable. The CIP fractions of those three force fields are all less than 1.1% (Table 2). While, for ff_DRVH and ff_KRLL, the PMF values of the CIP are comparable to those of SShIP and the transition energy barrier is around 12.5 kJ/mol, indicating both CIP and SShIP are stable. The CIP configuration fractions increased to 3.254% for ff_KRLL force field.

The fraction of CIP increased with temperature. When temperature increased to 523 K (Figs. 1b) and 773 K (Fig. 1c), the PMF values of CIP become smallest, which means CIP is the most stable configuration for all these force fields. Correspondingly, as temperature increases from ambient temperature to 523 K to 773 K, the CIP fraction of ff_FN grows up from 0.132% to 7.419% to 61.766%, and the CIP fraction in ff_KRLL grows up from 3.254% to 20.957% to 75.139%. The stability of the CIP configuration is increased with the increasing of temperature. This is primarily because of the lower values of dielectric constants of water as increasing temperature and decreasing density.

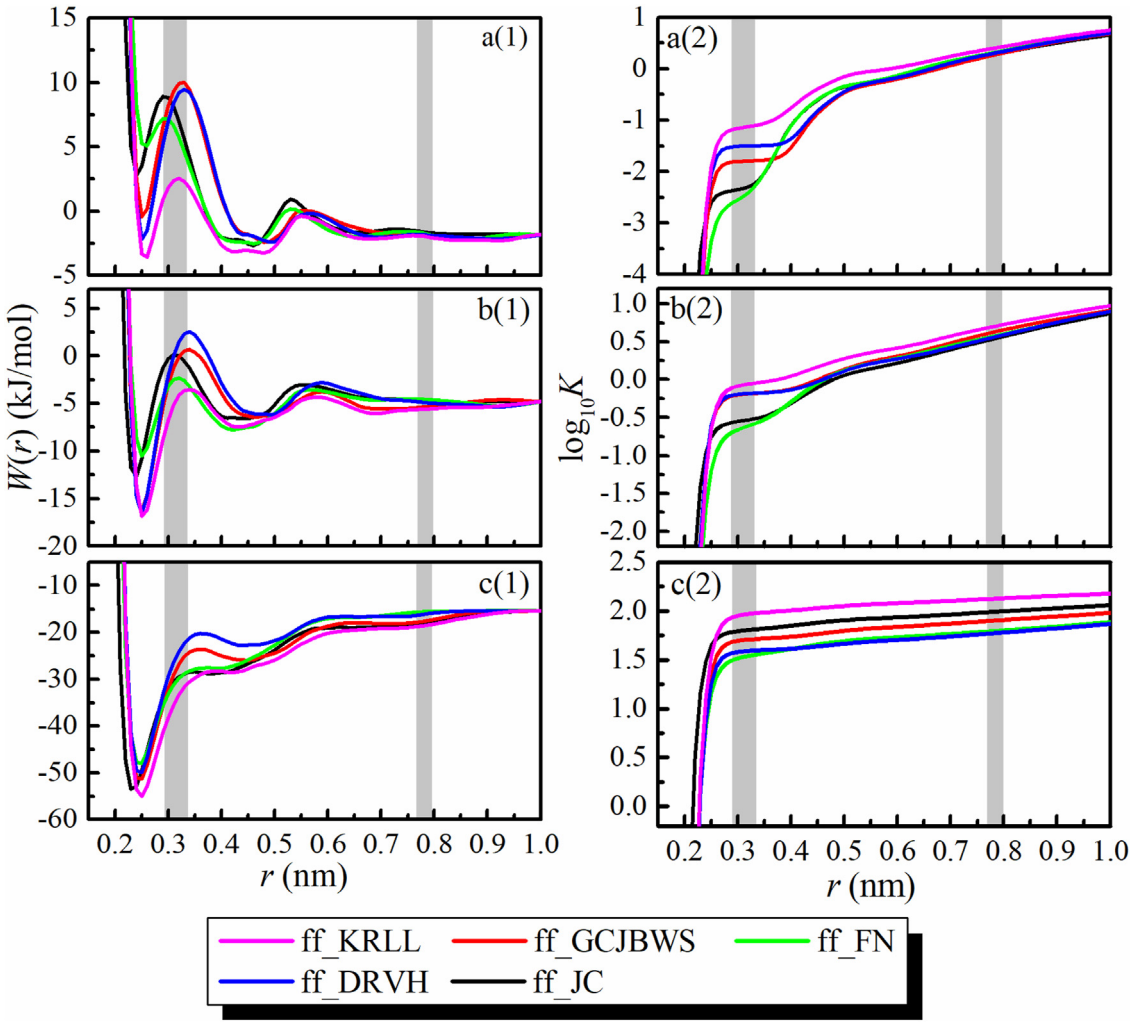

Fig. 1. The PMF profiles of Na^+–F^- ion-pair and corresponding $\log_{10}K_a(m)$ of these force fields at 298 K and 1 bar (a), 523 K and 500 bar (b), 773 K and 1000 bar (c).

Table 2
The logarithm of both $K_{CIP}(m)$ and $K_{all}(m)$ and mole fraction of CIP calculated using these force fields parameters.

	$\log_{10}K_{CIP}(m)$	$\log_{10}K_{all}(m)$	% mole CIP
$T = 298$ K $P = 1$ bar			
ff_FN	−2.606 ± 0.018	0.274 ± 0.059	0.132
ff_JC	−2.398 ± 0.036	0.151 ± 0.067	0.283
ff_GCJBWS	−1.796 ± 0.033	0.171 ± 0.097	1.080
ff_DRVH	−1.495 ± 0.010	0.302 ± 0.124	1.595
ff_KRLL	−1.125 ± 0.025	0.362 ± 0.109	3.254
$T = 523$ K $P = 500$ bar			
ff_FN	−0.609 ± 0.016	0.521 ± 0.227	7.419
ff_JC	−0.541 ± 0.045	0.519 ± 0.249	8.711
ff_GCJBWS	−0.176 ± 0.044	0.522 ± 0.311	20.036
ff_DRVH	−0.175 ± 0.026	0.491 ± 0.273	21.555
ff_KRLL	−0.039 ± 0.034	0.640 ± 0.245	20.957
$T = 773$ K $P = 1000$ bar			
ff_FN	1.584 ± 0.018	1.793 ± 0.078	61.766
ff_JC	1.820 ± 0.027	1.990 ± 0.273	67.603
ff_GCJBWS	1.720 ± 0.056	1.901 ± 0.334	65.991
ff_DRVH	1.602 ± 0.045	1.771 ± 0.235	67.705
ff_KRLL	2.000 ± 0.023	2.124 ± 0.129	75.139

3.2. RDF characteristics

Fig. 2 gives the radial distribution functions (RDFs) of Na−O (Fig. 2a) and F−H (Fig. 2b) from these force field parameters and the results from the AIMD calculation. The locations of the first peak for $g(r)_{Na-O}$ of these force fields are varying from 0.225 nm to 0.26 nm, and those for $g(r)_{F-H}$ ranging from 0.16 nm to 0.21 nm. It can be seen from Fig. 2b that the RDFs of F−H pair can be clearly divided into two groups. The group consist of ff_JC, ff_FN and ff_KRLL has a r_{F-H} first peak at 0.16 nm, and the first peak of group ff_DRVH and ff_GCJBWS is at ~0.2 nm. The r_{Na-O} first peak of ff_DRVH and ff_GCJBWS could still be placed into the same group at ~0.225 nm, while that for ff_JC, ff_FN and ff_ KRLL are a bit of scattered ranging from 0.24 nm to 0.26 nm.

The AIMD calculated first peak of $g(r)_{F-H}$ is located at 0.16 nm, and the first peak of $g(r)_{NaO}$ is situated at 0.225 nm, which is accord with previous *ab initio* studies [21,64,65]. Compared with the AIMD calculation, the r_{F-H} first peak of ff_JC, ff_FN, ff_KRLL is in a good agreement with the results of the AIMD calculation, and the r_{Na-O} first peak of ff_JC agreed very well with that of the AIMD calculation. The r_{Na-O} first peak of ff_FN and the ff_KRLL parameters were respectively 0.05 nm and 0.15 nm larger than that of the AIDM calculation.

3.3. Association constant

Association constant calculated with only CIP and with CIP + SShIP + SSIP are denoted as K_{CIP} and K_{all} respectively. For the calculation of K_{CIP}, the integration limit r_c in Eq. (3) is located at the position of the first maximum on the PMF profile, while for K_{all} it is the value at the position of the last maximum (the gray bar shown in Fig. 1). To compare the present calculation with the experimental data, the MD calculated molar-concentration-based association constants, $K_a(M)$ (L/mol), were converted into the molality-based $K_a(m)$ (kg/mol) by multiplying water density ρ, $K_a(m) = K_a(M)\cdot\rho$. The water density was in unit of g/cm^3 and calculated with equations of IAPWS-IF97 [66] at same temperature and pressure. The $\log_{10}K_a(m)$ were shown in the right part of Fig. 1 and listed in Table 2.

As we can see from Table 2 and Fig. 1, the $K_{all}(m)$ are always larger than $K_{CIP}(m)$. But this difference becomes smaller with increasing temperature, when CIP becoming the predominated speciation. As temperature increased from 298 K to 773 K, the $\log_{10}K$ difference between $K_{all}(m)$ and $K_{CIP}(m)$ decreased from 2.880 to 0.209 for the ff_FN, and from 1.488 to 0.124 for the ff_KRLL.

The $K_{all}(m)$ from different force fields are in a good agreement with each other and are within 0.35 log unit. But big variations are occurred for the CIP association constants among these force fields. The largest deviation is 1.481 at 298 K between ff_FN and ff_KRLL. As shown in the right part of Fig. 1 and Table 2, the bottom and top boundaries of $K_{CIP}(m)$ at the given thermodynamic conditions are the constants from ff_FN and ff_KRLL respectively.

At 298 K and 1 bar, the association constants $\log_{10}K_a(m)$ from literature varied from −0.959 to 0.38 [10,11,13,15,67]. The $\log_{10}K_{all}(m)$ calculated from all those force field parameters agreed well with the recently reported ones: 0.224 from Faridi and El Guendouzi [10] and 0.270 from Aghaie and Samaie [11], which indicates that the experimentally determined ion association speciation from Refs. [10,11] is more likely to be CIP + SShIP + SSIP. However, it is important to bear in mind that it is not a decisive conclusion. Association constants in Refs. [10,11] were determined from the

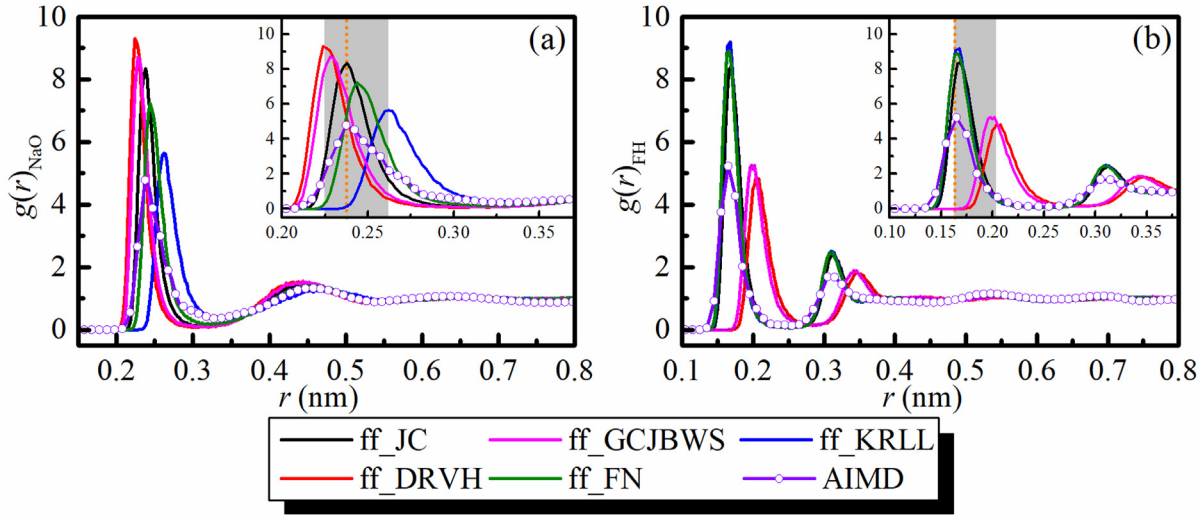

Fig. 2. The radial distribution functions patters of Na−O (a) and F−H (b) calculated from these force fields and the results from AIMD at 298 K and 1 bar.

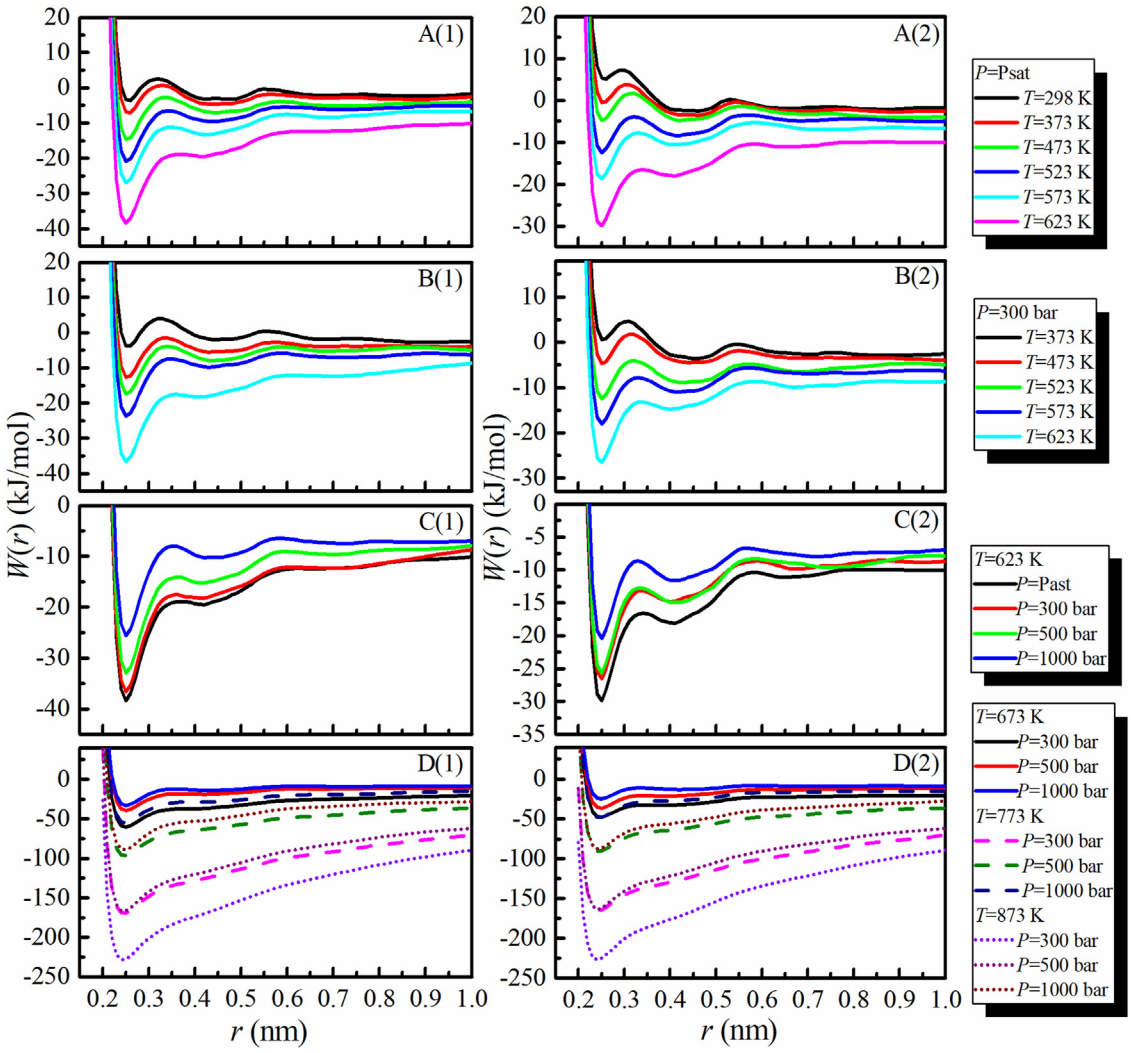

Fig. 3. The PMF profiles calculated at different temperature and pressure. Data from ff_KRLL are plotted on the left and those from ff_FN are on the right.

difference of NaF salt solubility product between experiment and standard Gibbs energy calculation. The actual associated configurations and the ratio of CIP or SShIP are not clear.

Figs. 1 and 2 shows that the PMF profiles and RDFs of Na−O and F−H calculated from these force fields varied widely from each other. Although the RDFs of Na−O and F−H calculated from ff_KRLL and ff_FN were similar, the CIP configuration is stable in ff_KRLL but not in ff_FN. The associated ion pair calculated from ff_JC, ff_FN and f_GCJBWS could be SShIP + SSIP as PMF values of CIP is higher and the transition energies from CIP to SShIP is lower. More accurate simulations with polarizable force fields, from AIMD or experiments are needed in future studies to figure out the exact configurations of the associated ion pair.

From the mentioned above, the PMFs and the corresponding $K_a(m)$ are force field sensitive especially for $K_{CIP}(m)$. The maxima and minima of the $K_{CIP}(m)$ from these force fields are settled by ff_KRLL and ff_FN. Combined with the RDFs provided in Fig. 2, the ff_KRLL and ff_FN force field parameters were selected for further calculation. The PMFs and $K_a(m)$ of Na^+−F^- ion-pair with 300, 518 and 1036 water molecules at 523 K and 500 bar are given in Fig. S2. It can be seen, the position of CIP, SShIP and SSIP was almost the same with each other, and the calculated association constants are within the uncertainties.

3.4. PMFs and association constants at high temperature and pressure

The PMF profiles calculated from ff_KRLL (left) and ff_FN (right) at different temperature and pressure are shown in Fig. 3. Na^+−F^- ion-pair tends to associate with increasing temperature and dissociate with increasing pressure. Fig. 3A, B and C show the PMF profiles under sub-supercritical conditions. When temperature increases, the PMF values of the CIP becomes smaller, and reaches the smallest point among those configurations at temperature over 473 K. At 623 K, when pressure increased from the saturated vapor pressure to 1000 bar, the CIP PMF value of ff_KRLL increased from −38.365 kJ/mol to −25.600 kJ/mol. And it increased from −29.894 kJ/mol to −20.393 kJ/mol for ff_FN. Fig. 3D gives PMF profiles in the supercritical conditions with pressure ranging from 300 bar to 1000 bar. It shows when pressure increased from 300 bar to 1000 bar at 873 K, the CIP PMF value increments are about 200 kJ/mol for both force field parameters.

The corresponding logarithmic of $K_{CIP}(m)$ and $K_{all}(m)$ at different temperature and pressure for both ff_FN and ff_KRLL are listed in Table 3 and fitted by using an empirical density model equation [37,41]:

Table 3
Logarithm of molar association constants of Na^+-F^- ion-pair from ff_FN and ff_KRLL for both $K_{CIP}(m)$ and $K_{all}(m)$.

T/K	P/bar	ff_FN		ff_KRLL	
		$\log_{10}K_{CIP}(m)$	$\log_{10}K_{all}(m)$	$\log_{10}K_{CIP}(m)$	$\log_{10}K_{all}(m)$
298	1	−2.606 ± 0.018	0.274 ± 0.059	−1.125 ± 0.025	0.362 ± 0.109
373	Psat	−1.562 ± 0.083	0.306 ± 0.258	−0.715 ± 0.015	0.465 ± 0.092
473	Psat	−1.165 ± 0.043	0.294 ± 0.293	−0.171 ± 0.027	0.625 ± 0.129
523	Psat	−0.518 ± 0.150	0.491 ± 0.235	0.251 ± 0.011	0.774 ± 0.043
573	Psat	−0.124 ± 0.036	0.621 ± 0.277	0.576 ± 0.064	0.973 ± 0.142
623	Psat	0.563 ± 0.061	1.038 ± 0.128	1.232 ± 0.021	1.442 ± 0.235
373	300	−1.698 ± 0.055	0.304 ± 0.237	−1.163 ± 0.045	0.225 ± 0.334
473	300	−1.167 ± 0.026	0.322 ± 0.149	−0.357 ± 0.027	0.488 ± 0.248
523	300	−0.505 ± 0.036	0.610 ± 0.105	−0.063 ± 0.063	0.607 ± 0.237
573	300	−0.150 ± 0.046	0.655 ± 0.356	0.303 ± 0.044	0.768 ± 0.125
623	300	0.338 ± 0.060	0.876 ± 0.299	1.135 ± 0.034	1.383 ± 0.245
623	500	0.294 ± 0.045	0.880 ± 0.245	0.874 ± 0.028	1.143 ± 0.077
623	1000	−0.082 ± 0.029	0.683 ± 0.136	0.303 ± 0.023	0.764 ± 0.198
673	300	1.575 ± 0.029	1.892 ± 0.209	2.468 ± 0.124	2.577 ± 0.358
673	500	0.868 ± 0.020	1.249 ± 0.055	1.068 ± 0.076	1.297 ± 0.294
673	1000	0.106 ± 0.018	0.735 ± 0.055	0.660 ± 0.013	0.973 ± 0.109
773	300	8.431 ± 0.015	8.456 ± 0.067	8.696 ± 0.021	8.704 ± 0.142
773	500	3.795 ± 0.046	3.883 ± 0.085	4.172 ± 0.011	4.211 ± 0.141
773	1000	1.584 ± 0.018	1.793 ± 0.078	2.000 ± 0.023	2.124 ± 0.129
873	300	10.700 ± 0.027	10.709 ± 0.223	10.792 ± 0.018	10.795 ± 0.233
873	500	7.202 ± 0.054	7.223 ± 0.124	7.388 ± 0.036	7.397 ± 0.173
873	1000	3.049 ± 0.128	3.131 ± 0.299	3.154 ± 0.133	3.198 ± 0.324

Table 4
Fitting parameters of Eq. (11) for the calculation of Na^+-F^- ion-pair logarithm molar association constants.

Parameters	ff_FN		ff_KRLL	
	$\log_{10}K_{CIP}(m)$	$\log_{10}K_{all}(m)$	$\log_{10}K_{CIP}(m)$	$\log_{10}K_{all}(m)$
a_1	−0.464	−1.47	−0.723	−1.345
a_2	−447.200	678.20	−40.730	642.900
a_3	−18.760	−20.07	−15.680	−17.030
a_4	7173	8592	4624	5940

$$\log_{10}K_a(m) = a_1 + \frac{a_2}{T} + \left(a_3 + \frac{a_4}{T}\right)\log_{10}\rho \tag{11}$$

where ρ is the density of pure water and calculated with equations of IAPWS-IF97 at temperature and pressure of interest, T is the absolute temperature. The fitted parameters (a_1~a_4) are listed in Table 4.

From Fig. 4 and Table 3, we can see that $K_{all}(m)$ from these two force field parameters are consistent with each other, within 0.4 log unit. But, the difference between $K_{CIP}(m)$ and $K_{all}(m)$ from the same force field in the sub-critical region is significant. For ff_FN, these $K_{CIP}(m)$ and $K_{all}(m)$ logarithmic differences are 2.002 at 373 K and 300 bar, a bit of decreased to 0.475 at 623 K and saturated vapor pressure, and to 0.538 at 623 K and 300 bar. For ff_KRLL, these differences are 1.387, 0.210 and 0.247, respectively, for the same condition of mentioned above. Moreover, significant differences of $K_{CIP}(m)$ between these force fields also occurred in the sub-critical region. $K_{CIP}(m)$ from ff_KRLL is always larger than that from ff_FN, and this difference is a bit of decreased with the increment of temperature. For the supercritical conditions, the two kinds of differences were decreased to within 0.3 log unit, when CIP becoming the predominate configurations.

Fig. 5 gives the indirect determined Na^+-F^- ion-pair association constants at 100 bar (Figs. 5a) and 300 bar (Fig. 5b) from Majer et al. [14], SUPCRT [68], and that calculated with the density model. It is interesting to note that K_a from SUPCRT are close to $K_{CIP}(m)$ from ff_KRLL. The association constants from Richardson and Holland [15] was the basis for SUPCRT. However, their association constants at 298 K (−0.959, adopted from Ref. [12]) varied much with the recently reported values (0.375 [67], 0.224 [10] and 0.270 [11]) and that from our study. Their $\log_{10}K_a$ values at high temperature, like 0.041 at 473 K and 0.544 at 533 K, fitted from fluorite solubility in NaCl solution, are in line with $K_{all}(m)$ from both ff_KRLL and ff_FN.

Compared with the AIMD RDF properties, the results of $g(r)_{NaO}$ and $g(r)_{FH}$ from the ff_FN is better, which indicates ff_FN would give the more accurate ion pairing properties. These is no directly experimental determined NaF association behaviors at high temperature and pressures. It is hard to say which force field parameters is better. And it does not matter much if it is only concerned with the association constant, since there is not much difference in K_{all} among those force field parameters. But if we consider the contact ion pair properties, like volumetric properties of Na^+-F^- ion-pair, much concern should be paid for the significance of CIP and the force field sensitivity of K_{CIP}. Fig. 6 depicts density maps representing distributions of water oxygen around Na^+ and F^- at the geometries of CIP, SShIP and SSIP calculated from ff_FN at 298 K and 1 bar. For the SSIP, the two solvent shells are largely independent of each other. For the SShIP, the single water molecule shared by the two ions. While for the CIP, this water molecule was replaced by the counterion, resulting in a marked asymmetry of the solvent shell, particularly for the smaller sodium ion. Thus, the volume of SShIP and SSIP seems to be the sum of the

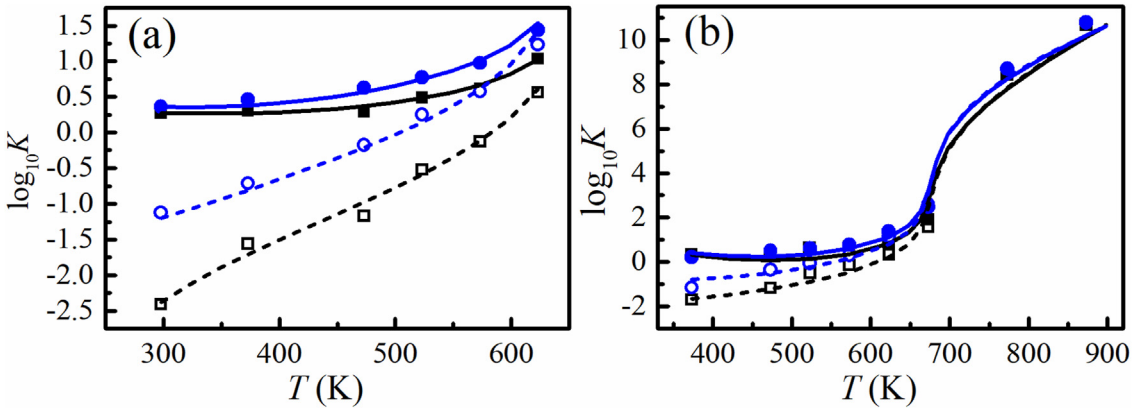

Fig. 4. The logarithm values of $K_{CIP}(m)$ and $K_{all}(m)$ for both ff_FN and ff_KRLL as a function of temperature at saturated vapor pressure (a) and $P = 300$ bar (b). The empty symbols represent CIP association constants $K_{CIP}(m)$, solid symbols are the CIP + SShIP + SSIP association constant $K_{all}(m)$. Black and blue lines refer to density model calculated ones with parameters from ff_FN and ff_KRLL, respectively. Short dash lines and solid lines are $K_{CIP}(m)$ and $K_{all}(m)$, respectively.

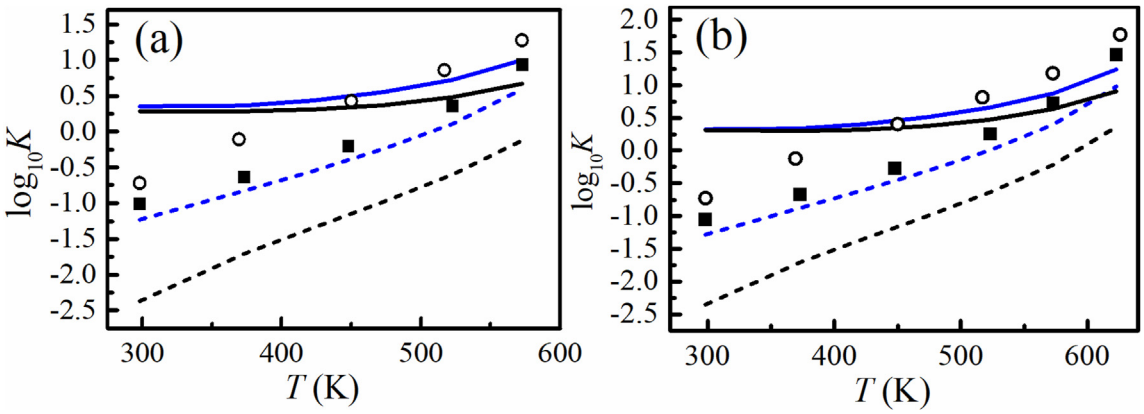

Fig. 5. The $\log_{10}K_a(m)$ values from literature and that calculated from density model at 100 bar (a) and 300 bar (b). The circle empty symbols represent Na^+–F^- ion-pair association constants from Majer et al. [14] and the solid square symbols are from SUPCRT [68]. Black and blue lines refer to the ff_FN and ff_KRLL, respectively. Short dash lines and solid lines are $K_{CIP}(m)$ and $K_{all}(m)$, respectively.

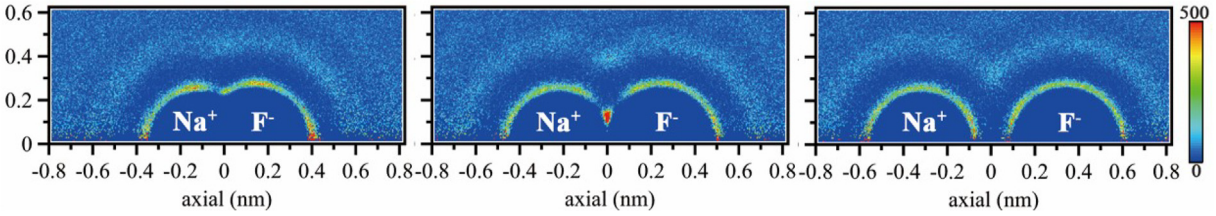

Fig. 6. Water density distributions around Na^+–F^- ion pair at CIP, SShIP and SSIP of ff_FN at 298 K and 1 bar.

volume of single ion and water molecules. But the volume additive procedure does not work for CIP. More accurate simulations from AIMD or experiments at high temperature and pressure are needed, especially for CIP formation.

4. Conclusion

NaF associations in dilute aqueous solutions have been extensively investigated through the constrained molecular dynamics simulations with five different force field parameters. The RDFs characteristics of Na^+ and F^- in water from these force field were compared with *ab initio* molecular dynamics at 298 K. The corresponding association constants of K_{CIP} and K_{all} were calculated from the PMFs. Three intermediate configurations of association of Na^+ and F^- (CIP, SShIP and SSIP) can be well identified with the local minima from the PMF profiles. The position, intensity and corresponding association constants of these configurations are force field sensitive. Force field parameters developed by combing single ion properties with mineral lattice energy or ion-pair interactions give better RDFs characteristics compared with the results from AIMD calculation. Na^+–F^- ion-pair tends to associate with increasing temperature and dissociate with increasing pressure. The molality based $K_{all}(m)$ calculated from all those force field parameters agree well with each other, and they are in accordance with the recently reported literature data at 298 K. However, In the sub-critical region, significant deviations occurred between the contact ion-pair association constants K_{CIP} and K_{all} for each force field and also between K_{CIP} for different force fields. These two kinds of differences are less than 0.4 log unit when CIP becoming the dominated configuration at the supercritical conditions.

Declaration of competing interest

The authors declare that they have no known competing financial interests or personal relationships that could have appeared to influence the work reported in this paper.

CRediT authorship contribution statement

Wei Zhang: Conceptualization, Methodology, Software, Supervision. **Tinggui Yan:** Methodology, Validation, Writing - review & editing.

Acknowledgements

This work was financially supported by the 2016 Doctoral Scientific Research Foundationof Guizhou Normal University, the Natural Science Foundation of Guizhou Province (LH [2017]7339, [2019]1230, [2019]1066), the National Natural Science Foundation of China (21808045), Guizhou Science and Technology platform talents ([2018]5781]) and Talent Introduction Fund of Guizhou University ([2017]23). We are truly grateful to the two anonymous reviewers' critical comments and thoughtful suggestions.

Appendix A. Supplementary data

Supplementary data to this article can be found online at https://doi.org/10.1016/j.fluid.2020.112615.

References

[1] A. Migdisov, A.E. Williams-Jones, J. Brugger, F.A. Caporuscio, Hydrothermal transport, deposition, and fractionation of the REE: experimental data and

thermodynamic calculations, Chem. Geol. 439 (2016) 13–42.
[2] S. Keshri, B.L. Tembe, Ion association in binary mixtures of water-CO_2 in supercritical conditions through classical molecular dynamics simulations, J. Mol. Liq. 257 (2018) 82–92.
[3] K. Yui, M. Sakuma, T. Funazukuri, Molecular dynamics simulation on ion-pair association of NaCl from ambient to supercritical water, Fluid Phase Equil. 297 (2010) 227–235.
[4] A. Plugatyr, R.A. Carvajal-Ortiz, I.M. Svishchev, Ion-pair association constant for LiOH in supercritical water, J. Chem. Eng. Data 56 (2011) 3637–3642.
[5] A.A. Chialvo, P.T. Cummings, J.M. Simonson, R.E. Mesmer, Molecular simulation study of speciation in supercritical aqueous NaCl solutions, J. Mol. Liq. 73–4 (1997) 361–372.
[6] A. Timofeev, A.A. Migdisov, A.E. Williams-Jones, An experimental study of the solubility and speciation of niobium in fluoride-bearing aqueous solutions at elevated temperature, Geochem. Cosmochim. Acta 158 (2015) 103–111.
[7] A.A. Migdisov, A.E. Williams-Jones, T. Wagner, An experimental study of the solubility and speciation of the Rare Earth Elements(III) in fluoride- and chloride-bearing aqueous solutions at temperatures up to 300 °C, Geochem. Cosmochim. Acta 73 (2009) 7087–7109.
[8] Y. Xing, B. Etschmann, W. Liu, Y. Mei, Y. Shvarov, D. Testemale, A. Tomkins, J. Brugger, The role of fluorine in hydrothermal mobilization and transportation of Fe, U and REE and the formation of IOCG deposits, Chem. Geol. 504 (2019) 158–176.
[9] J.R. Haas, E.L. Shock, D.C. Sassani, Rare earth elements in hydrothermal systems: estimates of standard partial molal thermodynamic properties of aqueous complexes of the rare earth elements at high pressures and temperatures, Geochem. Cosmochim. Acta 59 (1995) 4329–4350.
[10] J. Faridi, M. El Guendouzi, Study of ion-pairing and thermodynamic properties of sodium fluoride in aqueous solutions at temperatures from 298.15 to 353.15 K, J. Solut. Chem. 44 (2015) 2194–2207.
[11] M. Aghaie, E. Samaie, Non-ideality and ion-pairing in saturated aqueous solution of sodium fluoride at 25 °C, J. Mol. Liq. 126 (2006) 72–74.
[12] G.R. Miller, D.R. Kester, Sodium fluoride ion-pairs in seawater, Mar. Chem. 4 (1976) 67–82.
[13] S. Manohar, G. Atkinson, The effect of high pressure on the ion pair equilibrium constant of alkali metal fluorides: a spectrophotometric study, J. Solut. Chem. 22 (1993) 859–872.
[14] V. Majer, M. Obšil, G. Hefter, J.-P. Grolier, Volumetric behavior of aqueous NaF and KF solutions up to 350 °C and 30 MPa, J. Solut. Chem. 26 (1997) 847–875.
[15] C.K. Richardson, H.D. Holland, The solubility of fluorite in hydrothermal solutions, an experimental study, Geochem. Cosmochim. Acta 43 (1979) 1313–1325.
[16] W.J. Xie, Z. Zhang, Y.Q. Gao, Ion pairing in alkali nitrate electrolyte solutions, J. Phys. Chem. B 120 (2016) 2343–2351.
[17] E. Guàrdia, R. Rey, J.A. Padró, Na^+–Na^+ and Cl^-–Cl^- ion pairs in water: mean force potentials by constrained molecular dynamics, J. Chem. Phys. 95 (1991) 2823–2831.
[18] A.A. Chialvo, J.M. Simonson, Aqueous Na^+Cl^- pair association from liquid like to steam like densities along near-critical isotherms, J. Chem. Phys. 118 (2003) 7921–7929.
[19] J. Timko, D. Bucher, S. Kuyucak, Dissociation of NaCl in water from ab initio molecular dynamics simulations, J. Chem. Phys. 132 (2010) 114510.
[20] J.P. Larentzos, L.J. Criscenti, A molecular dynamics study of alkaline earth metal-chloride complexation in aqueous solution, J. Phys. Chem. B 112 (2008) 14243–14250.
[21] E. Pluhařová, O. Marsalek, B. Schmidt, P. Jungwirth, Ab initio molecular dynamics approach to a quantitative description of ion pairing in water, J. Phys. Chem. Lett. 6 (2015) 4177–4181.
[22] A.A. Siddique, M.K. Dixit, B.L. Tembe, Molecular dynamics simulations of Ca^{2+}–Cl^- ion pair in polar mixtures of acetone and water: solvation and dynamical studies, Chem. Phys. Lett. 662 (2016) 306–316.
[23] S. Keshri, R. Mandal, B.L. Tembe, Solvation structures and dynamics of alkaline earth metal halides in supercritical water: a molecular dynamics study, Chem. Phys. 476 (2016) 80–90.
[24] R.P. Matthews, K.J. Naidoo, Experimentally consistent ion association predicted for metal solutions from free energy simulations, J. Phys. Chem. B 114 (2010) 7286–7293.
[25] M. Xu, J.P. Larentzos, M. Roshdy, L.J. Criscenti, H.C. Allen, Aqueous divalent metal-nitrate interactions: hydration versus ion pairing, Phys. Chem. Chem. Phys. 10 (2008) 4793–4801.
[26] C.J. Fennell, A. Bizjak, V. Vlachy, K.A. Dill, Ion pairing in molecular simulations of aqueous alkali halide solutions, J. Phys. Chem. B 113 (2009) 6782–6791.
[27] R. Buchner, G.T. Hefter, J. Barthel, Dielectric relaxation of aqueous NaF and KF solutions, J. Chem. Soc., Faraday Trans. 90 (1994) 2475–2479.
[28] S. Koneshan, J.C. Rasaiah, R.M. Lynden-Bell, S.H. Lee, Solvent structure, dynamics, and Ion mobility in aqueous solutions at 25 °C, J. Phys. Chem. B 102 (1998) 4193–4204.
[29] H.J.C. Berendsen, J.R. Grigera, T.P. Straatsma, The missing term in effective pair potentials, J. Phys. Chem. 91 (1987) 6269–6271.
[30] B. Hess, C. Holm, N. van der Vegt, Osmotic coefficients of atomistic $NaCl_{(aq)}$ force fields, J. Chem. Phys. 124 (2006) 164509.
[31] A.P. Lyubartsev, A. Laaksonen, Osmotic and activity coefficients from effective potentials for hydrated ions, Phys. Rev. E 55 (1997) 5689–5696.
[32] I.S. Joung, T.E. Cheatham, Determination of alkali and halide monovalent ion parameters for use in explicitly solvated biomolecular simulations, J. Phys. Chem. B 112 (2008) 9020–9041.
[33] M.B. Gee, N.R. Cox, Y. Jiao, N. Bentenitis, S. Weerasinghe, P.E. Smith, A Kirkwood-Buff derived force field for aqueous alkali halides, J. Chem. Theor. Comput. 7 (2011) 1369–1380.
[34] J.G. Kirkwood, F.P. Buff, The statistical mechanical theory of solutions. I, J. Chem. Phys. 19 (1951) 774–777.
[35] M. Fyta, R.R. Netz, Ionic force field optimization based on single-ion and ion-pair solvation properties: going beyond standard mixing rules, J. Chem. Phys. 136 (2012) 124103.
[36] S. Deublein, J. Vrabec, H. Hasse, A set of molecular models for alkali and halide ions in aqueous solution, J. Chem. Phys. 136 (2012), 084501.
[37] A.A. Chialvo, P.T. Cummings, H.D. Cochran, J.M. Simonson, R.E. Mesmer, Na^+–Cl^- ion pair association in supercritical water, J. Chem. Phys. 103 (1995) 9379–9387.
[38] Y. Mei, W. Liu, J. Brugger, D.M. Sherman, J.D. Gale, The dissociation mechanism and thermodynamic properties of $HCl_{(aq)}$ in hydrothermal fluids (to 700 °C, 60 kbar) by ab initio molecular dynamics simulations, Geochem. Cosmochim. Acta 226 (2018) 84–106.
[39] Y. Mei, D.M. Sherman, W.H. Liu, J. Brugger, Ab initio molecular dynamics simulation and free energy exploration of copper(I) complexation by chloride and bisulfide in hydrothermal fluids, Geochem. Cosmochim. Acta 102 (2013) 45–64.
[40] Y. Mei, B. Etschmann, W. Liu, D.M. Sherman, S.J. Barnes, M.L. Fiorentini, T.M. Seward, D. Testemale, J. Brugger, Palladium complexation in chloride- and bisulfide-rich fluids: insights from ab initio molecular dynamics simulations and X-ray absorption spectroscopy, Geochem. Cosmochim. Acta 161 (2015) 128–145.
[41] Z. Zhang, Z. Duan, Lithium chloride ionic association in dilute aqueous solution: a constrained molecular dynamics study, Chem. Phys. 297 (2004) 221–233.
[42] A.A. Chialvo, J.M. Simonson, $H3O^+Cl^-$ Pair association in steam and highly compressible aqueous environments, J. Phys. Chem. C 111 (2007) 15569–15574.
[43] A.A. Chialvo, P.C. Ho, D.A. Palmer, M.S. Gruszkiewicz, P.T. Cummings, J.M. Simonson, H_3O^+/Cl^- association in high-temperature aqueous solutions over a wide range of state conditions. A Direct comparison between simulation and electrical conductance experiment, J. Phys. Chem. B 106 (2002) 2041–2046.
[44] A.A. Chialvo, P.T. Cummings, J.M. Simonson, R.E. Mesmer, Temperature and density effects on the high temperature ionic speciation in dilute Na^+/Cl^- aqueous solutions, J. Chem. Phys. 105 (1996) 9248–9257.
[45] J. Van Eerden, W.J. Briels, S. Harkema, D. Feil, Potential of mean force by thermodynamic integration: molecular-dynamics simulation of decomplexation, Chem. Phys. Lett. 164 (1989) 370–376.
[46] A. Plugatyr, I.M. Svishchev, Accurate thermodynamic and dielectric equations of state for high-temperature simulated water, Fluid Phase Equil. 277 (2009) 145–151.
[47] Q. Zhang, R. Zhang, Y. Zhao, H.H. Li, Y.Q. Gao, W. Zhuang, Pairing preferences of the model mono-valence mono-atomic ions investigated by molecular simulation, J. Chem. Phys. 140 (2014) 1346.
[48] M.J. Abraham, T. Murtola, R. Schulz, S. Páll, J.C. Smith, B. Hess, E. Lindahl, GROMACS: high performance molecular simulations through multi-level parallelism from laptops to supercomputers, Software 1–2 (2015) 19–25.
[49] S. Reiser, S. Deublein, J. Vrabec, H. Hasse, Molecular dispersion energy parameters for alkali and halide ions in aqueous solution, J. Chem. Phys. 140 (2014), 044504.
[50] S. Miyamoto, P.A. Kollman, SETTLE: an analytical version of the SHAKE and RATTLE algorithm for rigid water models, J. Comput. Chem. 13 (1992) 952–962.
[51] B. Hess, H. Bekker, H.J.C. Berendsen, J.G.E.M. Fraaije, LINCS: a linear constraint solver for molecular simulations, J. Comput. Chem. 18 (1997) 1463–1472.
[52] W.F. Van Gunsteren, H.J.C. Berendsen, A leap-frog algorithm for stochastic dynamics, Mol. Simulat. 1 (1988) 173–185.
[53] W.G. Hoover, Canonical dynamics: equilibrium phase-space distributions, Phys. Rev. A 31 (1985) 1695–1697.
[54] G.J. Martyna, M.L. Klein, M. Tuckerman, Nosé–Hoover chains: the canonical ensemble via continuous dynamics, J. Chem. Phys. 97 (1992) 2635–2643.
[55] M. Parrinello, A. Rahman, Polymorphic transitions in single crystals: a new molecular dynamics method, J. Appl. Phys. 52 (1981) 7182–7190.
[56] U. Essmann, L. Perera, M.L. Berkowitz, T. Darden, H. Lee, L.G. Pedersen, A smooth particle mesh Ewald method, J. Chem. Phys. 103 (1995) 8577–8593.
[57] J. VandeVondele, M. Krack, F. Mohamed, M. Parrinello, T. Chassaing, J. Hutter, Quickstep: fast and accurate density functional calculations using a mixed Gaussian and plane waves approach, Comput. Phys. Commun. 167 (2005) 103–128.
[58] A.D. Becke, Density-functional exchange-energy approximation with correct asymptotic behavior, Phys. Rev. A 38 (1988) 3098–3100.
[59] C. Lee, W. Yang, R.G. Parr, Development of the colle-salvetti correlation-energy formula into a functional of the electron density, Phys. Rev. B 37 (1988) 785–789.
[60] S. Grimme, J. Antony, S. Ehrlich, H. Krieg, A consistent and accurate ab initio parametrization of density functional dispersion correction (DFT-D) for the 94 elements H-Pu, J. Chem. Phys. 132 (2010) 154104.
[61] J. VandeVondele, J. Hutter, Gaussian basis sets for accurate calculations on molecular systems in gas and condensed phases, J. Chem. Phys. 127 (2007)

114105.
[62] S. Goedecker, M. Teter, J. Hutter, Separable dual-space Gaussian pseudopotentials, Phys. Rev. B 54 (1996) 1703.
[63] M.P. Allen, D.J. Tildesley, Computer Simulation of Liquids, Oxford university press, 1987.
[64] H. Ma, Hydration structure of Na^+, K^+, F^-, and Cl^- in ambient and supercritical water: a quantum mechanics/molecular mechanics study, Int. J. Quant. Chem. 114 (2014) 1006–1011.
[65] J.M. Heuft, E.J. Meijer, Density functional theory based molecular-dynamics study of aqueous fluoride solvation, J. Chem. Phys. 122 (2005), 094501.
[66] W. Wagner, A. Kruse, H.-J. Kurtzschmar, Properties of Water and Steam: the Industrial Standard IAPWS-IF97 for the Thermodynamic Properties and Supplementary Equations for Other Properties: Tables Based on These Equations, Springer-Verlag Berlin, 1998.
[67] E.V. Lukyanova, A.V. Zotov, Determination of the $NaF_{(aq)}$ association constant for the NaF–NaCl–H_2O System at 25–75 °C by means of potentiometry, Russ. J. Phys. Chem. 91 (2017) 672–677.
[68] J.W. Johnson, E.H. Oelkers, H.C. Helgeson, SUPCRT92: a software package for calculating the standard molal thermodynamic properties of minerals, gases, aqueous species, and reactions from 1 to 5000 bar and 0 to 1000 °C, Comput. Geosci. 18 (1992) 899–947.